DETECTION OF TERRACETTES IN SEMI-ARID RANGELANDS USING FOURIER-BASED IMAGE ANALYSIS OF VERY HIGH-RESOLUTION SATELLITE IMAGERY

A Thesis

Presented in Partial Fulfillment of the Requirements for the

Degree of Master of Science

with a

Major in Water Resources

in the

College of Graduate Studies

University of Idaho

by

Ian N. Hellman

Major Professor: Robert Heinse, Ph.D.

Committee Members: Mark Corrao, Ph.D.; Jason Karl, Ph.D.

Department Administrator: Matthew Morra, Ph.D.

May 2020

Authorization to Submit Thesis

This thesis of Ian N. Hellman, submitted for the degree of Master of Science with a Major in Water Resources and titled "Detection of Terracettes in Semi-Arid Rangelands Using Fourier-Based Image Analysis of Very High-Resolution Satellite Imagery," has been reviewed in final form. Permission, as indicated by the signatures and dates below, is now granted to submit final copies to the College of Graduate Studies for approval.

Major Professor: _____ Date: _____
Robert Heinse, Ph.D.

Committee Members: _____ Date: _____
Mark Corrao, Ph.D.

_____ Date: _____
Jason Karl, Ph.D.

Department Administrator: _____ Date: _____
Matthew Morra, Ph.D.

Abstract

Terracettes, a step-like microtopographic feature primarily caused by livestock hoof action and grazing on hillslopes, are found throughout semi-arid rangelands of the United States. They have been shown to alter soil moisture, sediment transport, infiltration rates, and coincident vegetation patterns. The spatial extent of terracettes is currently unknown and therefore their landscape-scale hydrologic influence is absent in modeling and land management decision making. When viewed in very high-resolution satellite imagery, terracettes appear as repetitious parallel lines within a specific frequency range. Here, we use frequency-based image analysis via the 2D Discrete Fourier Transform to detect terracettes based on their distinct patterning and orientation. An automated workflow was created to detect terracettes using freely available software and satellite imagery. Results show a detection accuracy of 77%.

Acknowledgements

I would like to thank my advisor Dr. Robert Heinse for his advice, patience, and for allowing me the freedom to explore this topic in my own way. My committee members Dr. Jason Karl and Dr. Mark Corrao provided great insight and assistance through this process and for that, I thank them. Additionally, I would like to thank all of the other faculty, staff, and fellow students for their help and good times. Finally, I want to thank my wife Cody for her unwavering support along this journey.

Table of Contents

List of Figures

List of Tables

1. Introduction

Hillslope hydrologic processes play an important role in surface water runoff, sediment transport, nutrient availability, groundwater recharge, and stream flow (Cook, 1946; Dunne et al., 1991; Horton, 1933). The efficacy of these processes has been shown to be dramatically affected by topography and vegetation (Bergkamp, 1998; Hawkins & Cundy, 1987). A dramatic example of altered hillslope topography is the terracette, a step like, microtopographic feature found on rangeland hillslopes around the world (Buckhouse & Krueger, 1981; Corrao et al., 2015; Jin et al., 2016; Kück & Lewis, 2002; Walsh et al., 2001; Watanabe, 1994). Despite their global distribution and common occurrence on non-forested hillslopes in a range of climates, there is no comprehensive land cover inventory of terracettes. In the U.S. State of Idaho, Corrao et al. (2015) estimated 159,000 ha of terracetted hillslopes using point sampling and ocular analysis of orthoimagery. Other than this study, there have been few attempts to map terracettes beyond the hillslope scale. This paper describes a semi-automated algorithm to identify and map terracettes on a regional to global scale.

Accurately identifying terracettes on a landscape scale may aid in many uses for land cover data including land use change (Jennings, 2000; Lawler et al., 2014; USDA, 2013), land management for forage production (Holechek et al., 1999), and hydrologic model parameterization (Nearing et al., 2011). Livestock may be the dominant geomorphic agents of terracette formation in semi-arid systems (Walsh et al., 2001; Watanabe, 1994) but some have found solifluction to be the driving factor (Bielecki & Mueller, 2002; Buckhouse & Krueger, 1981; Kück & Lewis, 2002). Livestock preferentially use these pathways compacting the benches and therefore reducing vegetation (Jin et al., 2016; Stavi et al., 2008). The increased hillslope roughness due to terracettes may promote more infiltration and reduce runoff through increased ponding on benches (Hawkins & Cundy, 1987) and preferential infiltration paths from vegetation on the shoulder of the bench (Bergkamp, 1998). Much of the previous work on terracettes reference the effect of microtopographic features on hillslope processes. However, because all previous studies have focused on

single-hillslope functions and processes, their implications at larger spatiotemporal scales have been limited.

The fields of image processing and computer vision have enabled the analysis of the 'texture' of an image based on pixel intensity differences and patterns (Gonzalez & Woods, 2006). The 2-dimensional discrete Fourier transform (DFT), a technique for analyzing repeating patterns in imagery, is used widely across disciplines. The DFT has proven useful for detecting periodic, linear features from imagery by decomposing the complex, periodic signals into the individual frequencies (Couteron et al., 2006; Gonzalez & Woods, 2006; Mugglestone & Renshaw, 1998). Looking at the intensity, or prevalence, of a range of frequencies, Mugglestone & Renshaw (1998) were able to identify frequency patterns in aerial images corresponding to linear glacial landforms. Couteron et al. (2006) used what they termed Fourier-based Textural Ordination (FOTO) to classify the texture of a scene using radial spectral averages in principal component analysis. Because terracettes present as periodic, parallel, linear features when viewed in satellite or aerial imagery, we hypothesized that a Fourier-based approach may be well suited to automatically detecting terracettes.

Typically, terracettes are only resolvable in very high-resolution imagery (<0.5m ground sampling distance, i.e., resolution). However, for DFT analysis only relative intensity differences in the periodic features of the image are needed. Thus, the use and combination of uncalibrated RGB imagery from multiple sensors is possible (Mugglestone & Renshaw, 1998). Publicly available aerial imagery is well suited for this due to its high resolution and large spatial coverage. The DFT's tolerance for even heavily processed, pan-sharpened RGB imagery and its widely demonstrated ability to identify periodic features (Moisan, 2011; Smith, 1997; Xu, 1996) makes it ideal for identifying terracettes.

The objective of this study was to develop and apply a DFT rule-based classification of high-resolution aerial imagery to map terracettes and assess classification accuracy at kilometric scales using three study areas in Idaho and Washington, USA.

2. Materials and Methods

2.1. Study Area and Field Description

We selected three study areas (Wilma Ranch, Asotin, and Riggins) in the semi-arid region of northern Idaho and southeastern Washington (Figure 1). Each site was selected for having a wide variety of land use and topographic characteristics based on ocular examination of aerial imagery. The dominant land uses were farming and grazing on private land. All areas contained distinct valley bottoms, steep slopes and were typified by a mostly dendritic drainage network pattern. Bedrock at all sites was dominated by Columbia River basalts and soils were predominantly gravelly to cobbly silt loams. Thirty-year (1981-2010) mean precipitation, December mean temperatures, and July mean temperatures for all sites ranged from 381 to 460mm, -1.7 to 0.4C, and 20.7 to 22.1C, respectively. Elevation above sea level for all sites ranged from 225m to 1420m. Vegetation cover on non-cropland was mostly grasses and shrubs with some larger woody vegetation in valley bottoms and northern aspect slopes.

2.2. Imagery and Data Inputs

All imagery used was georeferenced aerial images of approximately 15cm resolution. The Wilma and Asotin sites were imaged on June 15, 2015 and the Riggins site on July 30, 2016. Imagery for the study area was available only as 3-band red, green, blue (RGB) "true color" images. The RGB bands were averaged together giving a single band raster with grey-scale values ranging from 0-255. All sites, Wilma Ranch (45 km^2), Asotin (56 km^2), and Riggins (16 km^2), were split into 1 km^2 subscenes. Each subscene was broken into non-overlapping windows of ~37x37 m (250x250 pixels). A window size of 250x250 pixels was selected for two reasons: First, it was large enough to provide sufficient repetitions of terracettes in the imagery following Couteron's (2006) suggestion that fine-grained patterns should repeat more than 3-4 times in each window for DFT. Second, because terracettes are very fine-grained patterns at the available resolution, a sufficiently small window size increases the continuity of terracette patterns in each window and increases the likelihood that they appear as linear parallel features even if they are part of a larger, curved set in complex terrain.

A USGS 10m DEM (U.S. Geological Survey, 2017) was used to create slope (degrees) and aspect (degrees) derivatives for all sites. Slope was used for masking out slopes below 5° and above 60° and aspect was used for site characterization of classification results. The 2011 National Land Cover Database (NLCD) (Homer et al., 2015) was used for masking out areas where terracettes were unlikely to exist (e.g. urban areas and water bodies) and where we would be unable to identify them in the unlikely situation that they exist (e.g. forests). For this study, we limited selection to the two classes of Grassland/Herbaceous and Shrub/Scrub. The NLCD 2011 is based primarily on a decision-tree classification of circa 2011 Landsat satellite data and has an overall land-cover class accuracy of 83% (Wickham et al., 2017).

2.3. Fourier Frequency Analysis

The primary goal of the Fourier frequency analysis was to extract dominant frequency and orientation exhibited in each window (Figure 2). Dominant frequency and orientation values were subsequently used as inputs for classification. The Fast Fourier Transform (FFT) (Diggle, 1990) function in the R software package (R Core Team, 2017) was used to calculate the DFT for each window. This converts the intensity values ($0 \leq I \leq 255$) in the spatial domain to the frequency domain. Image values of I(x,y) where x and y are the position of a pixel are transposed to Fourier-space values F(p,q) where p and q are spatial frequencies along XY directions (Proisy, Couteron, & Fromard, 2007). All image information in this transformation is preserved and editable in the frequency domain, readily allowing the extraction of periodic features (Figure 3). The underlying values calculated by the FFT are complex numbers representing the phase and magnitude. While the phase determines the main content of an image, the magnitude has been shown to contain the information related to periodic patterns (Jahne, 2004). Therefore, for this study, only the magnitude portion of the transformation was kept. The result of each transformed window calculated was a two-dimensional periodogram (Figure 4) displaying the distribution of spectral radiance periodicity at all spatial frequencies, or wavenumbers *r* where *r* was defined as the number of times a signal repeated itself in an image (Mugglestone & Renshaw, 1998). Wavelength can be determined by dividing the dimension of the square image by wavenumber. Here, *r* was expressed as cycles per meter. The periodogram was used as the

source of spectral data to determine the dominant frequency and orientation. All extracted values from the periodogram of each window were added to a single table for the classification process.

2.3.1. Frequency

The dominant spatial frequency of a window is represented by the largest magnitude value in the periodogram. Couteron (2002) suggested ignoring the magnitudes of the first two lowest frequencies as they represent the macro-heterogeneity of the image. To accomplish this with windows of a higher pixel count used here, the lowest five values are ignored. The position of the maximum magnitude value in the periodogram is found and by determining this position and corresponding wavenumber, we know the dominant frequency. This position value is added to the table of all window observations.

2.3.2. Orientation

The dominant orientation of a Fourier-space image, if present, is expressed as higher magnitude values or clusters of values perpendicular to the features in the original RGB image (Figure 4). By finding the clustering of higher magnitude values, we can determine the orientation. A directional raster (with values between 0 and 179 degrees) was created so that equal directions have equal values (e.g. the orientation of 20° is the same as 200°). We then use this raster to calculate zonal statistics (mean) of magnitude values for all directions in each window. A loess smoothing function (Cleveland & Devlin, 1988) is applied to the magnitude values when plotted as a function of orientation. Using a peak finding function the largest peak, or dominant orientation, is recorded into the table of all window observations.

2.4. Window Classification

A rule-based classification approach was used to classify each window. The rules were optimized based on manual assessment of a random sample of windows from all study sites. The final classification represents whether each window was independently classified as having terracettes or not having terracettes.

2.4.1. Validation Data

Validation data for the classification was collected via ocular assessment of randomly selected windows in all test scenes. First, approximations of terracette coverage at all sites were digitized into binary classification polygon shapefiles with terracette and non-terracette classes. A random sampling of 200 windows from each class was used to select the individual windows to be classified. Each window was examined at full resolution and given a binary value for terracette presence or absence. A total of 1,180 windows were manually examined to provide the validation data used in the classification, of which 316 were determined to contain terracettes. The final validation data used for classification was balanced by random selection so that both classes had an equal number of samples.

2.4.2. Determining Optimal Parameters

The validation data was used to determine the best combination of observed image frequency and image orientation that resulted in the most accurate classification of terracettes. This was performed through an iterative process which works through all combinations of these two parameters to find an optimal spatial frequency range in validation data terracettes. When viewed in orthoimagery, not all terracettes exhibited the same horizontal spacing between benches but tended to be within a narrow range (1-3 m). For the orientation we expected the observed, dominant orientation of a window containing terracettes to be perpendicular to the terracette feature. Because terracettes were expected to be roughly perpendicular to the aspect of the hillslope, window orientation values that were within an acceptable range of the DEM derived likely contain terracettes. For each combination of the two parameters, spatial frequency and orientation, a confusion matrix was generated using the validation data. The balanced accuracy and Cohen's kappa (Cohen, 1960) statistics were returned for each combination. Balanced accuracy is the average of the accuracies for both positive and negative classes (Brodersen et al., 2010). Cohen's kappa is a measure of how closely the observed instances matched the predicted instances while controlling for a random classification. This determination was performed separately for each study area as well as with all areas combined. The optimal parameters were then used to classify the full set of windows in each scene. The final classification was binary. Two classification schemes were tested for the final analysis. The first, frequency-only, was based solely on the

dominant frequency of each window and if it was within the range of acceptable frequencies. The second, frequency plus orientation, added an orientation rule and determined if the calculated dominant orientation of the window was within a defined angular bandwidth compared to the DEM derived aspect.

3. Results

3.1. Classification Accuracy

A total of 172,856 windows (117 km^2) were processed across all three study areas. Out of all the windows processed, 17,734 (12 km^2) were predicted to contain frequencies and orientations characteristic of terracettes. When analyzing each of the three study areas individually the frequency-only based classification had accuracies ranging from 0.76 to 0.77 and kappa values from 0.51 to 0.54 (Table 1). The frequency + orientation classification had accuracies from 0.76 to 0.78 and kappa values from 0.53 to 0.57, suggesting little benefit of including orientation information. The range between acceptable *r* values (wavenumbers) was 0.21 to 0.35 m^{-1} for the lower values and 0.67-1.88 m^{-1} for the upper values. When all sites were analyzed as one dataset, the parameters that produced the highest balanced accuracy and kappa values (0.77 and 0.53, respectively) were a lower *r* of 0.30 m^{-1}, upper *r* of 0.70 m^{-1} and angular bandwidths ranging from 50 to 60 degrees. The angular bandwidth is a range rather than a single value. The range stems from multiple combinations of angular bandwidths, lower *r* values, and upper *r* values that resulted in the exact same accuracy and kappa values. Therefore, our results suggest that a window has a higher likelihood of containing terracettes if the dominant, calculated wavenumber *r* is between the lower and upper *r* values and is oriented +/- 50-60 degrees of the DEM derived aspect.

In Figure 6, the effect of the lower and upper *r* values can be seen. For the lower *r*, an increase in kappa values from 0 to 0.30 m^{-1} with a peak at 0.32 m^{-1}. After this, there is a steep drop in kappa values. For the upper *r*, we see an increase in kappa from 0 to 0.67 m^{-1} and a leveling off to the maximum allowed *r*. Values below 0.30 m^{-1} are features with lower frequencies, or larger features in the RGB image that repeat fewer times in each window. Values above 0.67 m^{-1} are features that are smaller than terracettes and at the resolution of

images used in this study characterizes very fine grained, inter-pixel intensity differences. When looking at the influence of the angular bandwidth on kappa values (Figure 7), we found a subtle peak near 50-60. This again suggests that the orientation information used here did not greatly contribute to increased classification accuracy.

3.2. Classification Characteristics

Characteristics for each terracette and non-terracette window were determined for both the validation data and final classification of each study area. For aspect, terracettes were predominantly on north, northeast, and northwest facing slopes (Figure 8). This was true for the validation data as well as the final classification. Non-terracettes were slightly more evenly distributed, if not more prominent on the southern facing slopes. The non-terracettes in the Wilma area were predominantly on southern facing slopes. Slope was much more uniform between the terracette and non-terracette classification. Both the validation data and final classification showed very similar distributions of terracette and non-terracette windows (Figure 9). Mapping the final classification in a GIS (Figure 10), the terracettes clearly exhibited clustering.

4. Discussion

The application of Fourier-based classification used here proves to be a simple and therefore potentially powerful tool for identifying terracettes. These methods do not require calibrated imagery and only rely on basic, open source software functions. This reduces the cost and provides an opportunity to explore larger spatial extents. Knowing the location of terracettes can then be used to aid in hydrologic modeling, rangeland management, and resource inventory.

The spatial coverage values for each study area in Table 2 suggest that terracettes are a prominent feature in semi-arid rangelands. The area deemed suitable for terracette development, based on slope and land cover, was 77.8 km^2 (66.5%) in all sites combined. The manually identified terracetted zones totaled 8.9 km^2 (8.2%) of the total combined area studied and the final DFT classification shows 12.0 km^2 (11.5%) of terracetted land. The current spatial coverage of this study doesn't allow for reasonable extrapolation from these

values to larger scales. However, the methodology used here combined with random, kilometric-scale plot sampling across state-wide or greater scales may further refined values like those of Corrao et al. (2015).

In order for the method applied here to work, high-resolution imagery is necessary to provide the detail and contrast needed to identify terracette patterns. High-resolution imagery (sub-meter) is becoming more available through a combination of an increasing network of acquisition platforms and online data repositories (e.g. Planet Team, 2019). Currently, some county-scale imagery in the United States is available with 15cm resolution (e.g. INSIDE Idaho, 2019).

The other significant limitation of this method is the timing of the imagery (Figure 11). Date of image capture and the resultant sun angle at that time can both help and hinder the visibility of terracettes by changing the contrast between terracette bench and riser features. Areas with lower incident sunlight angles (e.g. north facing slopes in the northern hemisphere) increase shadows and therefore contrast. Areas on southern facing slopes with more direct sunlight have lower contrast and as a result terracettes are not nearly as pronounced in the imagery. This may result in a potential underestimation of terracettes overall and possibly account for an increased estimation of terracettes on north facing aspects. This is likely a difficult problem to overcome but potentially solvable by variable image capture times. For aspect, our final classification results were consistent with Corrao et al. (2017) with north as the dominant aspect where terracettes are found. Further exploration of window size should be considered as this presents a variable in need of optimization.

The driving force behind the final classification is the manual, binary classification of the validation data. However, terracettes are a continuous land-cover feature that exist along a gradient ranging from very distinct to barely discernible. Powell et al. (2004) found that accurately labeling continuous landscapes was difficult due to inherent subjectivity. This was especially true when trying to label transitional classes. In this study, we assigned each window a binary classification. Therefore, we were unable to properly classify the areas of

transitional terracettes due to sub-window heterogeneity. When assessing the final classification of the validation points, the primary source of commission/omission errors (Table 1) appears to be from either faint terracettes or transitional classes. The method used here is also susceptible to commission errors due to windows exhibiting the same spatial frequency and orientation as terracettes but are indeed not terracettes. Future research on terracette classification should investigate using more classes, refining objective metrics for each class, and alternative windowing. A third, transitional class may bring attention to marginal or oddly shaped terracettes. Objective classification metrics such as a minimum number of terracettes of a certain length in the window would help reduce the inherent human subjectivity. Finally, incorporating overlapping windows may increase the identification of transitional terracettes as well as increase the confidence of all classifications.

Prior to this study, the spatial extent of terracettes was aggregated at the state level. While this certainly provides insight into statewide rangeland management, determining the precise locations of terracettes may allow for more tailored management strategies. Fuhlendorf et al., (2017) suggests a framework of functional heterogeneity which asks what type of heterogeneity, at various scales, is related to a process of interest. With the fine-grained knowledge of terracette location, future research may be able to discern the various hydrologic influence of terracettes at varying spatial scales. Without detailed knowledge of the spatial extent of terracettes our ability to infer their influence is limited (Seyfried & Wilcox, 1995). Site-specific observations, like those made by Bergkamp (1998) and Corrao et al. (2016), when used in conjunction with hillslope to watershed scale extent of terracettes, can help further inform the influence of terracettes in rangeland hydrology. This information matched with local soil and vegetation data may also aid in predicting forage production and therefore potential stocking densities. The hydrologic influence of terracettes may also be better understood when matched with their precise, spatial attributes (e.g. slope, aspect, elevation, etc.) that can be extracted from the final classification results.

5. Conclusion

Fourier-based image processing and classification methods are one approach to identifying terracettes across kilometric spatial extents and are limited primarily by imagery. The methods applied tolerate variable input imagery sources but are dependent on contrast in the terracette features. Timing of imagery and aspect may play a large role in estimating the amount of identified terracettes. This classification approach shows promise in determining the currently unquantified extent of terracettes. The results from our three study sites corroborate that terracettes are a widespread microtopographic feature in semi-arid rangelands. Our results suggest that they are more prevalent on north facing slopes although this may be exaggerated by the timing of image capture. While at least some degree of hillslope steepness is required for terracettes to occur, it does not appear to be the driving factor in terracette formation in arid rangelands. With the methods put forth here, it may be possible to explore the influence of terracettes on hillslope hydrologic processes at larger spatial scales and therefore increase the impact of rangeland focused management decisions.

6. References

Bergkamp, G. (1998). A hierarchical view of the interactions of runoff and infiltration with vegetation and microtopography in semiarid shrublands. *Catena*, *33*(3–4), 201–220. https://doi.org/10.1016/S0341-8162(98)00092-7

Bielecki, A. E., & Mueller, K. J. (2002). Origin of terraced hillslopes on active folds in the southern San Joaquin Valley, California. *Geomorphology*, *42*(1–2), 131–152. https://doi.org/10.1016/S0169-555X(01)00082-4

Brodersen, K. H., Ong, C. S., Stephan, K. E., & Buhmann, J. M. (2010). The balanced accuracy and its posterior distribution. *Proceedings - International Conference on Pattern Recognition*, 3121–3124. https://doi.org/10.1109/ICPR.2010.764

Buckhouse, J., & Krueger, W. (1981). What Caused Those Terracettes?. *Rangelands Archives*, *3*(2), 72–73.

Cleveland, W. S., & Devlin, S. J. (1988). Locally weighted regression: An approach to regression analysis by local fitting. *Journal of the American Statistical Association*, *83*(403), 596–610. https://doi.org/10.1080/01621459.1988.10478639

Cohen, J. (1960). A Coefficient of Agreement for Nominal Scales. *Educational and Psychological Measurement*, *20*(1), 37–46. https://doi.org/10.1177/001316446002000104

Cook, H. L. (1946). The infiltration approach to the calculation of surface runoff. *Eos, Transactions American Geophysical Union*, *27*(5), 726–747. https://doi.org/10.1029/TR027i005p00726-2

Corrao, M. V., Cosens, B. E., Heinse, R., Eitel, J. U. H., & Link, T. E. (2015). Using science to bridge management and policy: Terracette hydrologic function and water quality best management practices in Idaho. *Rangelands*, *37*(5), 191–199. https://doi.org/10.1016/j.rala.2015.08.003

Corrao, M. V., Heinse, R., Eitel, J. U. H., Cosens, B. E., & Link, T. E. (2016). Soil Moisture Differences between Terracette Benches and Risers on Semiarid Rangeland Hillslopes. *Vadose Zone Journal*, *15*(1), 1–10. https://doi.org/10.2136/vzj2015.04.0058

Corrao, M. V., Link, T. E., Heinse, R., & Eitel, J. U. H. (2017). Modeling of terracette-hillslope soil moisture as a function of aspect, slope and vegetation in a semi-arid environment. *Earth Surface Processes and Landforms*. https://doi.org/10.1002/esp.4114

Couteron, P. (2002). Quantifying change in patterned semi-arid vegetation by Fourier analysis of digitized aerial photographs. *International Journal of Remote Sensing*, *23*(17), 3407–3425. https://doi.org/10.1080/01431160110107699

Couteron, P., Barbier, N., & Gautier, D. (2006). Textural ordination based on fourier spectral decomposition: A method to analyze and compare landscape patterns. *Landscape Ecology*, *21*(4), 555–567. https://doi.org/10.1007/s10980-005-2166-6

Diggle, P. J. (1990). *Time Series: A Biostatistical Introduction*. Oxford [England] : New York, Claredon Press; Oxford University Press.

Dunne, T., Zhang, W., & Aubry, B. F. (1991). Effects of Rainfall, Vegetation, and Microtopography on Infiltration and Runoff. *Water Resources Research*, *27*(9), 2271–2285. https://doi.org/10.1029/91WR01585

Fuhlendorf, S. D., Fynn, R. W. S., McGranahan, D. A., & Twidwell, D. (2017). Heterogeneity as the Basis for Rangeland Management. In *Rangeland Systems, processes, Management and challenges* (pp. 169–196). https://doi.org/10.1007/978-3-319-46709-2_5

Gonzalez, R. C., & Woods, R. E. (2006). *Digital Image Processing (3rd Edition)*. Upper Saddle River, NJ, USA: Prentice-Hall, Inc.

Hawkins, R. H., & Cundy, T. W. (1987). Steady-State Analysis of Infiltration and Overland Flow for Spatially-Varied Hillslopes. *JAWRA Journal of the American Water Resources Association*, *23*(2), 251–256. https://doi.org/10.1111/j.1752-1688.1987.tb00804.x

Holechek, J. L., Gomez, H., Molinar, F., & Galt, D. (1999). Grazing Studies: What We've Learned Description by Grazing Region Forage Production and Stocking Rate Grazing Intensity: What is Moderate Stocking? *Rangeland*, *21*(2), 12–16. Retrieved from https://pdfs.semanticscholar.org/7584/3fbe08a4b1aaffb9faf88e2a78fcfd678acc.pdf

Homer, C. G., Dewitz, J., Yang, L., Jin, S., Danielson, P., Xian, G. Z., … Megown, K. (2015). Completion of the 2011 National Land Cover Database for the conterminous United States – Representing a decade of land cover change information. *Photogrammetric Engineering and Remote Sensing*, *81*, 345–354. Retrieved from http://pubs.er.usgs.gov/publication/70146301

Horton, R. E. (1933). The Role of infiltration in the hydrologic cycle. *Eos, Transactions American Geophysical Union*, *14*(1), 446–460. https://doi.org/10.1029/TR014i001p00446

INSIDE Idaho. (2019). Interactive Numeric & Spatial Information Data Engine (INSIDE) Idaho. Moscow, ID. www.insideidaho.org. Retrieved from insideidaho.org

Jahne, B. (2004). *Practical Handbook on Image Processing for Scientific and Technical Applications*. CRC Press. https://doi.org/10.1201/9780849390302

Jennings, M. D. (2000). Gap analysis: concepts , methods , and recent results. *Landscape Ecology*, *15*, 5–20.

Jin, B., Sun, G., Zhang, Y., Zou, M., Ni, X., Luo, K., … Wu, X. Ben. (2016). Livestock tracks transform resource distribution on terracette landscapes of the Loess Plateau. *Ecosphere*, *7*(4), 1–14. https://doi.org/10.1002/ecs2.1337

Kück, K. M., & Lewis, C. A. (2002). Terracettes and active gelifluction terraces in the drakensberg of the province of the eastern cape, south africa: A process study. *South African Geographical Journal*, *84*(2), 214–225. https://doi.org/10.1080/03736245.2002.9713773

Lawler, J. J., Lewis, D. J., Nelson, E., Plantinga, A. J., Polasky, S., Withey, J. C., …

Radeloff, V. C. (2014). Projected land-use change impacts on ecosystem services in the United States. *Proceedings of the National Academy of Sciences*, *111*(20), 7492–7497. https://doi.org/10.1073/pnas.1405557111

Moisan, L. (2011). Periodic plus smooth image decomposition. *Journal of Mathematical Imaging and Vision*, *39*(2), 161–179. https://doi.org/10.1007/s10851-010-0227-1

Mugglestone, M. A., & Renshaw, E. (1998). Detection of geological lineations on aerial photographs using two-dimensional spectral analysis. *Computers and Geosciences*, *24*(8), 771–784. https://doi.org/10.1016/S0098-3004(98)00065-X

Nearing, M. A., Wei, H., Stone, J. J., Pierson, F. B., Spaeth, K. E., Weltz, M. A., … Hernandez, M. (2011). A rangeland hydrology and erosion model. *Transactions of the ASABE*, *54*(3), 901–908.

Planet Team. (2019). Planet Application Program Interface: In Space for Life on Earth. San Francisco, CA. Retrieved from https://api.planet.com

Powell, R. L., Matzke, N., De Souza, C., Clark, M., Numata, I., Hess, L. L., … Roberts, D. A. (2004). Sources of error in accuracy assessment of thematic land-cover maps in the Brazilian Amazon. *Remote Sensing of Environment*, *90*(2), 221–234. https://doi.org/10.1016/j.rse.2003.12.007

Proisy, C., Couteron, P., & Fromard, F. (2007). Predicting and mapping mangrove biomass from canopy grain analysis using Fourier-based textural ordination of IKONOS images. *Remote Sensing of Environment*, *109*(3), 379–392. https://doi.org/10.1016/j.rse.2007.01.009

R Core Team. (2017). R: A Language and Environment for Statistical Computing. Vienna, Austria. Retrieved from http://www.r-project.org/

Seyfried, M. S., & Wilcox, B. P. (1995). Scale and the Nature of Spatial Variability: Field Examples Having Implications for Hydrologic Modeling. *Water Resources Research*, *31*(1), 173–184. https://doi.org/10.1029/94WR02025

Smith, S. W. (1997). The scientist and engineer's guide to digital signal processing.

Stavi, I., Ungar, E. D., Lavee, H., & Sarah, P. (2008). Surface microtopography and soil penetration resistance associated with shrub patches in a semiarid rangeland. *Geomorphology*, *94*(1–2), 69–78. https://doi.org/10.1016/j.geomorph.2007.05.008

U.S. Geological Survey. (2017). 1/3rd arc-second Digital Elevation Models (DEMs) - USGS

National Map 3DEP Downloadable Data Collection.

USDA. (2013). *Summary Report: 2010 National Resources Inventory (Natural Resources Conservation Service)*. Washington, DC.

Walsh, Collins, J. F., Guinan, L., Clavin, D. J., & Nixon, D. (2001). *Physical impact of livestock on the hill environment*.

Watanabe, T. (1994). Soil Erosion on Yak-Grazing Steps in the Langtang Himal, Nepal. *Mountain Research and Development*, *14*(2), 171–179. https://doi.org/10.2307/3673799

Wickham, J., Stehman, S. V., Gass, L., Dewitz, J. A., Sorenson, D. G., Granneman, B. J., … Baer, L. A. (2017). Thematic accuracy assessment of the 2011 National Land Cover Database (NLCD). *Remote Sensing of Environment*, *191*, 328–341. https://doi.org/10.1016/j.rse.2016.12.026

Xu, B. (1996). Identifying Fabric Structures with Fast Fourier Transform Techniques. *Textile Research Journal*, *66*(8), 496–506. https://doi.org/10.1177/004051759606600803

7. Figures

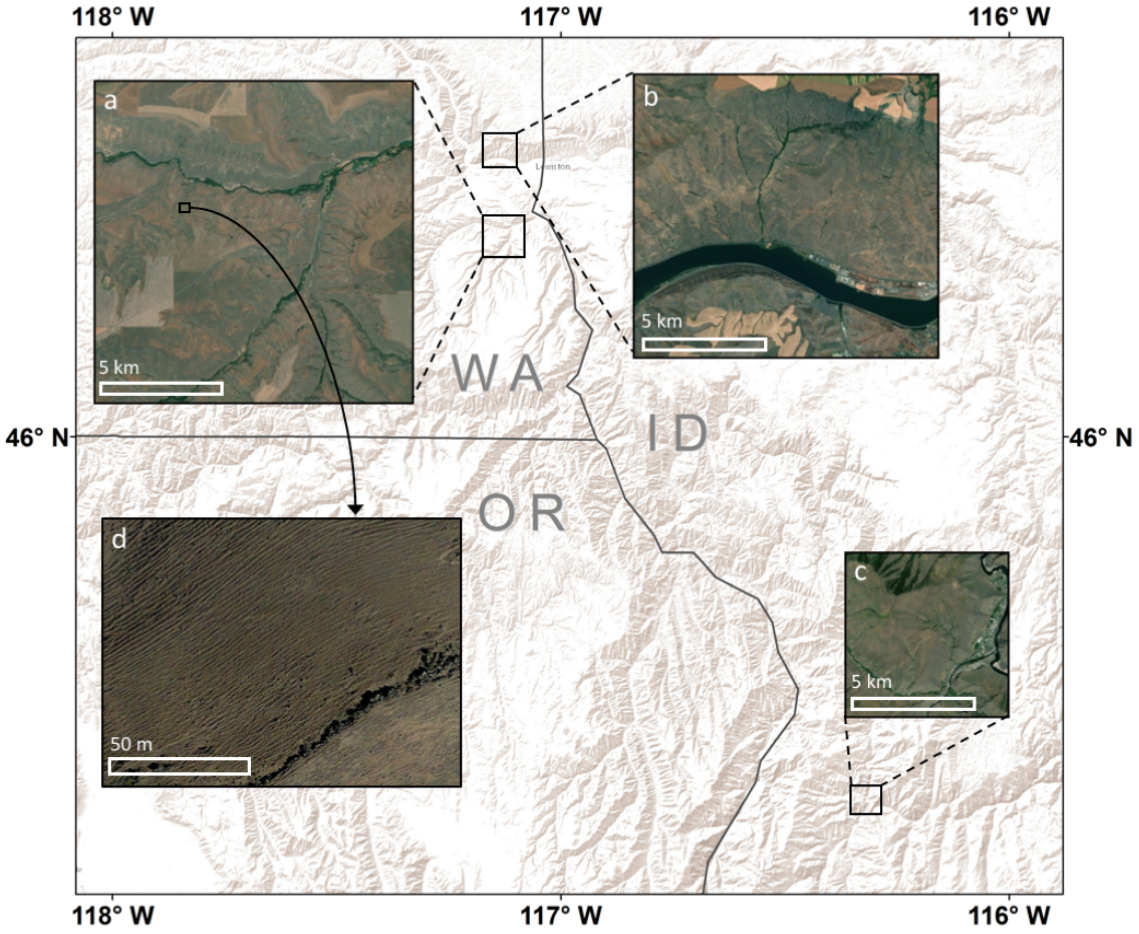

Figure 1. Overview map showing (a) Asotin, (b) Wilma Ranch, (c) Riggins study sites and (d) a typical hillslope with terracettes.

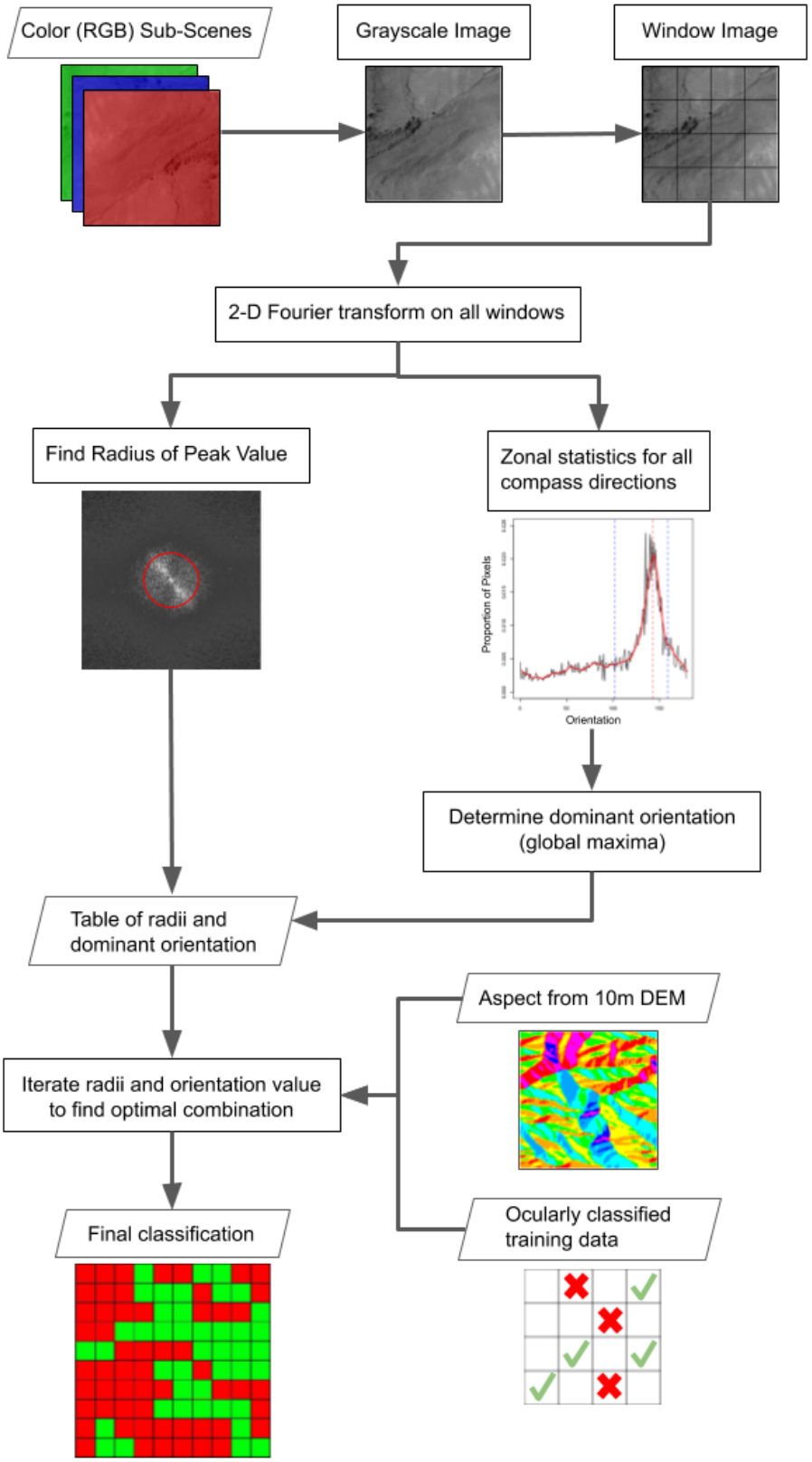

Figure 2. Flow diagram showing steps in Fourier-based classification.

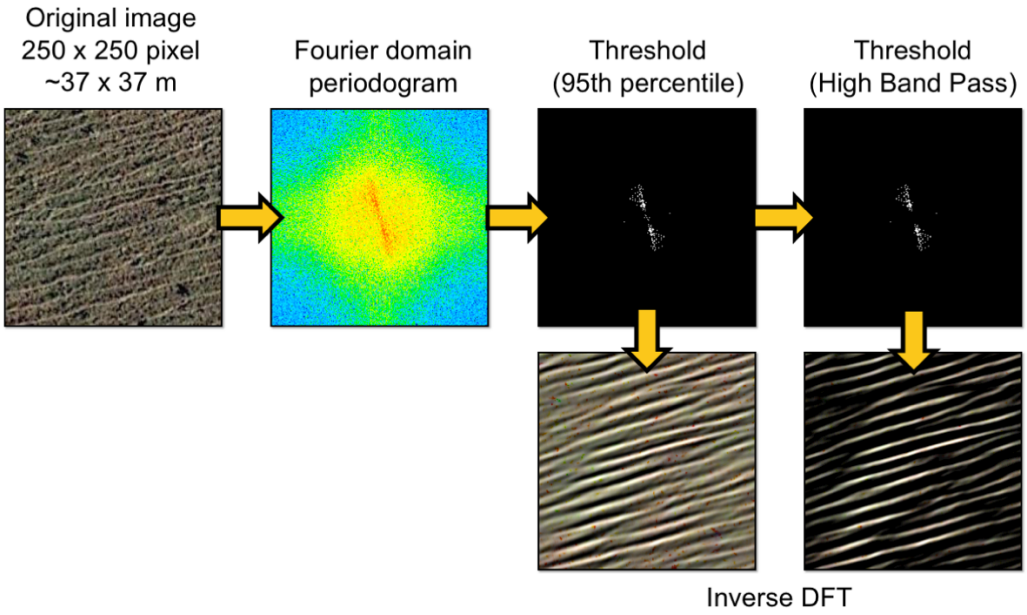

Figure 3. The image information, once in the Fourier frequency domain, still contains all image information and remains editable. Thresholding and applying a bandpass allows a visualization of the terracette information within the image.

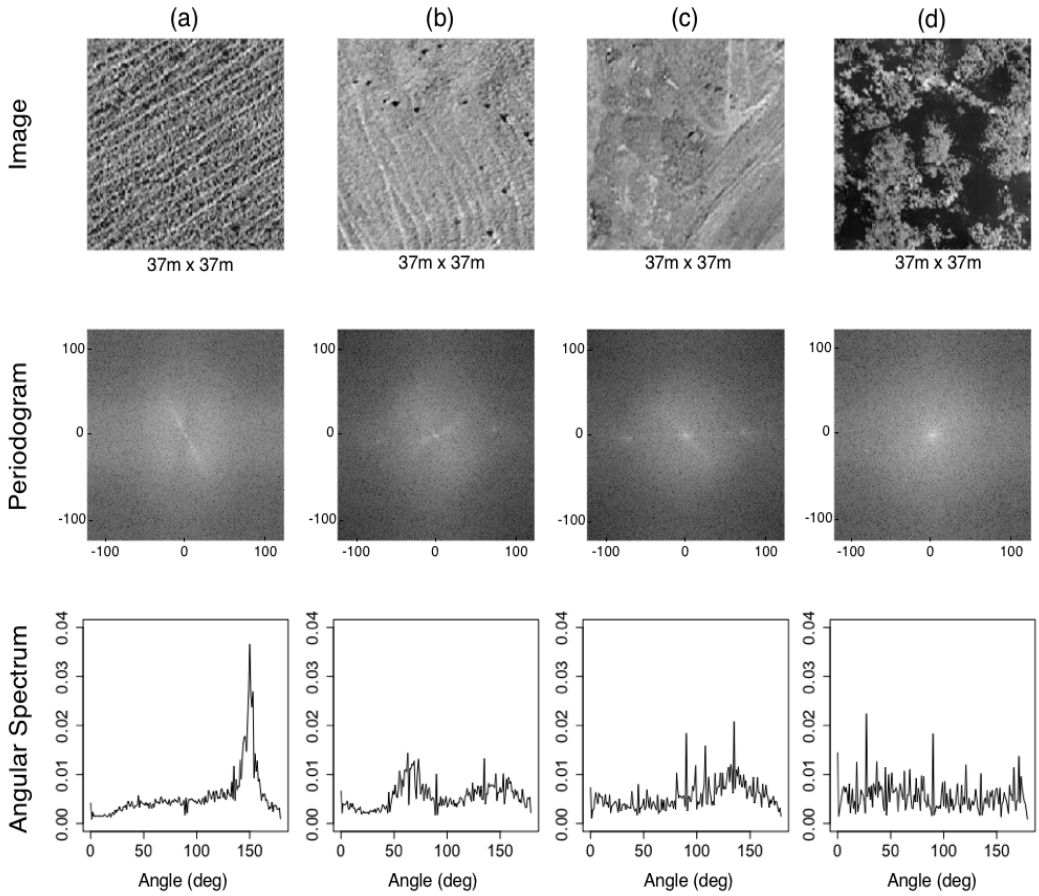

Figure 4. Example spectral attributes of individual windows in the Wilma Ranch study area. All images are oriented to the North. The periodograms are grayscale representations of FFT magnitude transformed so that $r = 0$ is at plot center. (a) Very distinct terracettes. (b) Faint, transitional terracettes. (c) Typical rangeland. (d) Forested.

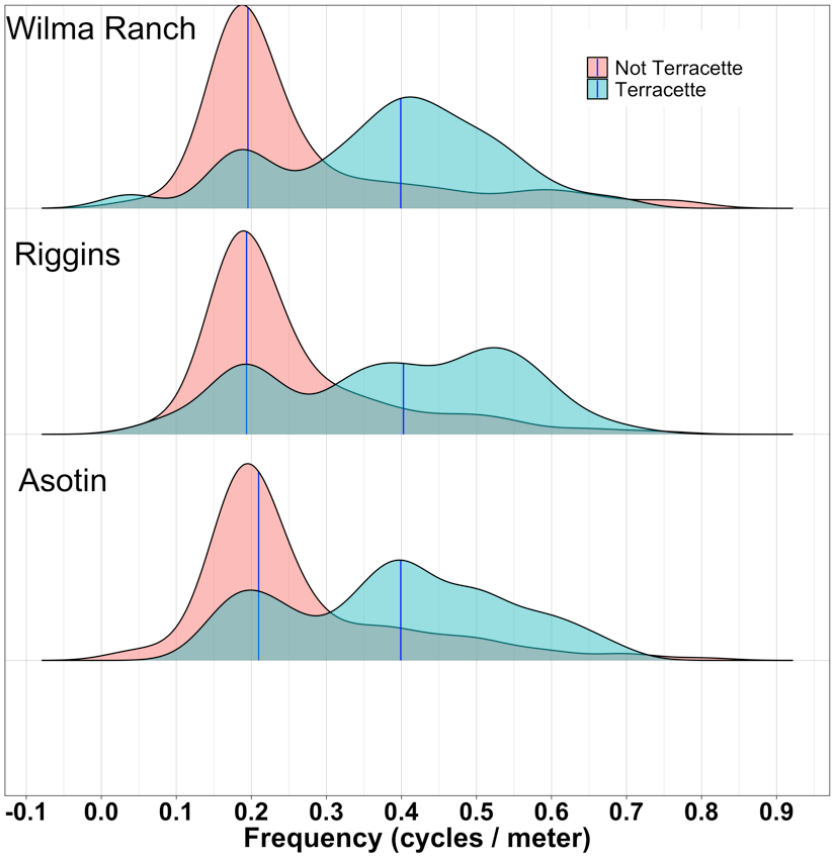

Figure 5. Density of the frequency of each validation data window. Non-terracette windows are dominated by lower frequencies likely due to larger scale features such as trees or change in vegetation. Terracette windows tend to have higher frequencies due to their unique pattern on the landscape.

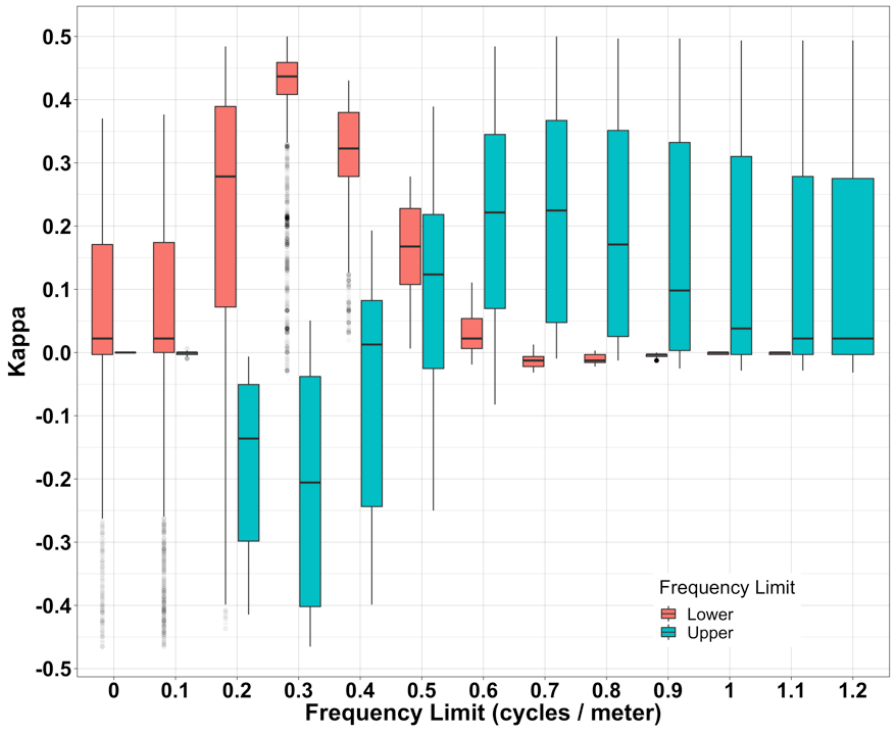

Figure 6. Kappa values for upper and lower frequency limits from the validation data. Each distribution represents the resultant kappa values for all combinations of angular bandwidth, the fixed frequency limit of that distribution, and all frequencies of the other limit (either Lower or Upper). Frequencies have been binned into nearest 0.1 m^{-1} for plotting.

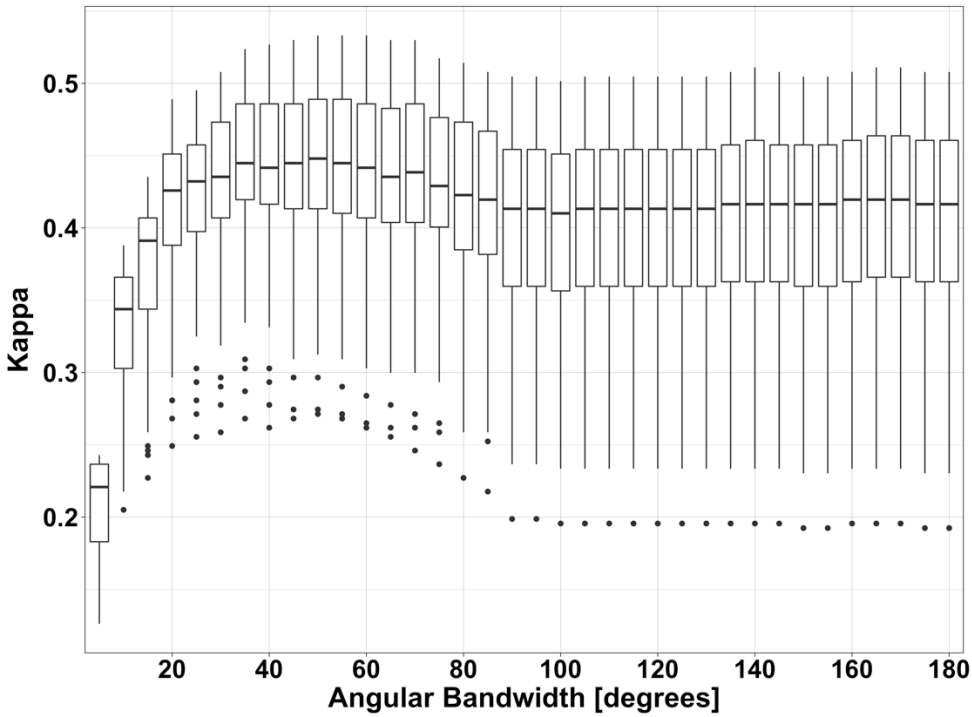

Figure 7. Kappa value ranges for angular bandwidths. Data shown is limited to lower frequency limits of 0.2-0.4m^{-1} and upper frequency limits of 0.5-0.8m^{-1}. Each angular bandwidth distribution represents the resultant kappa values for all combinations of lower frequency limit and upper frequency limit at that angular bandwidth.

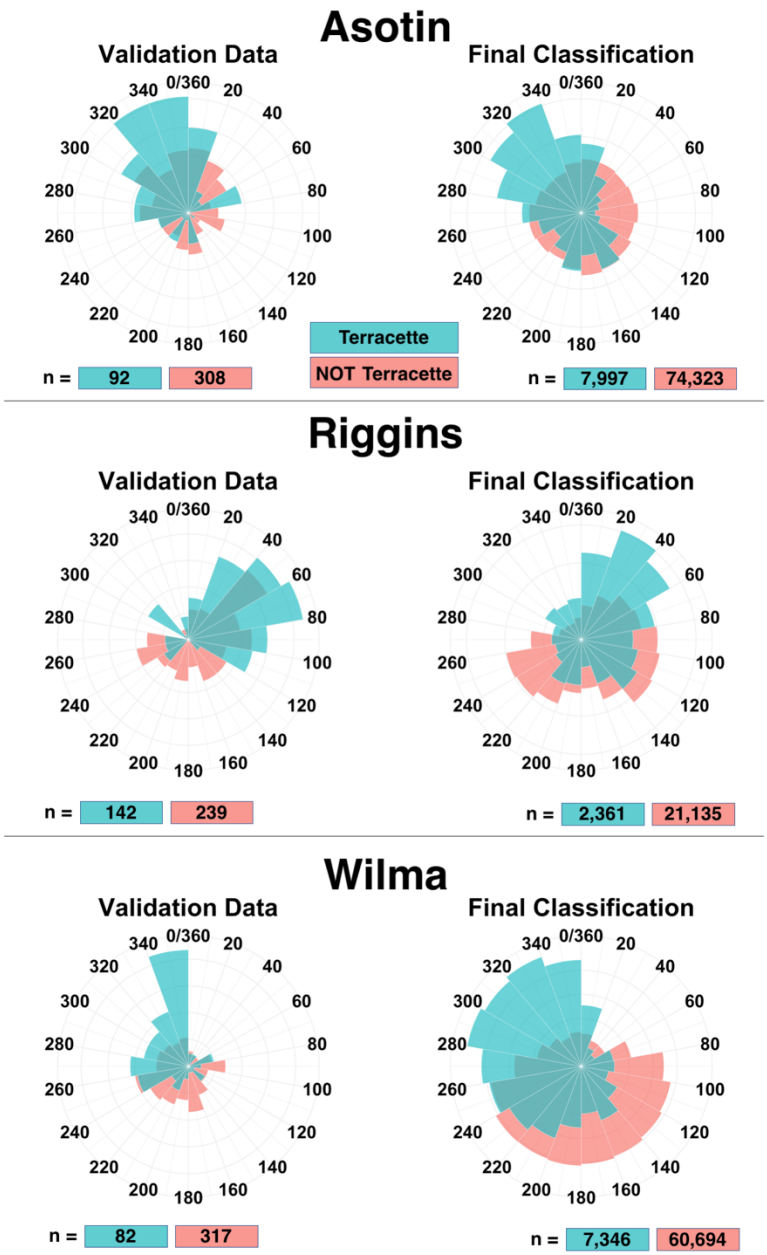

Figure 8. Density of window aspect for validation data and final classification. Aspects values were derived from a 10m DEM at each window centroid. Values below each diagram are the number of windows.

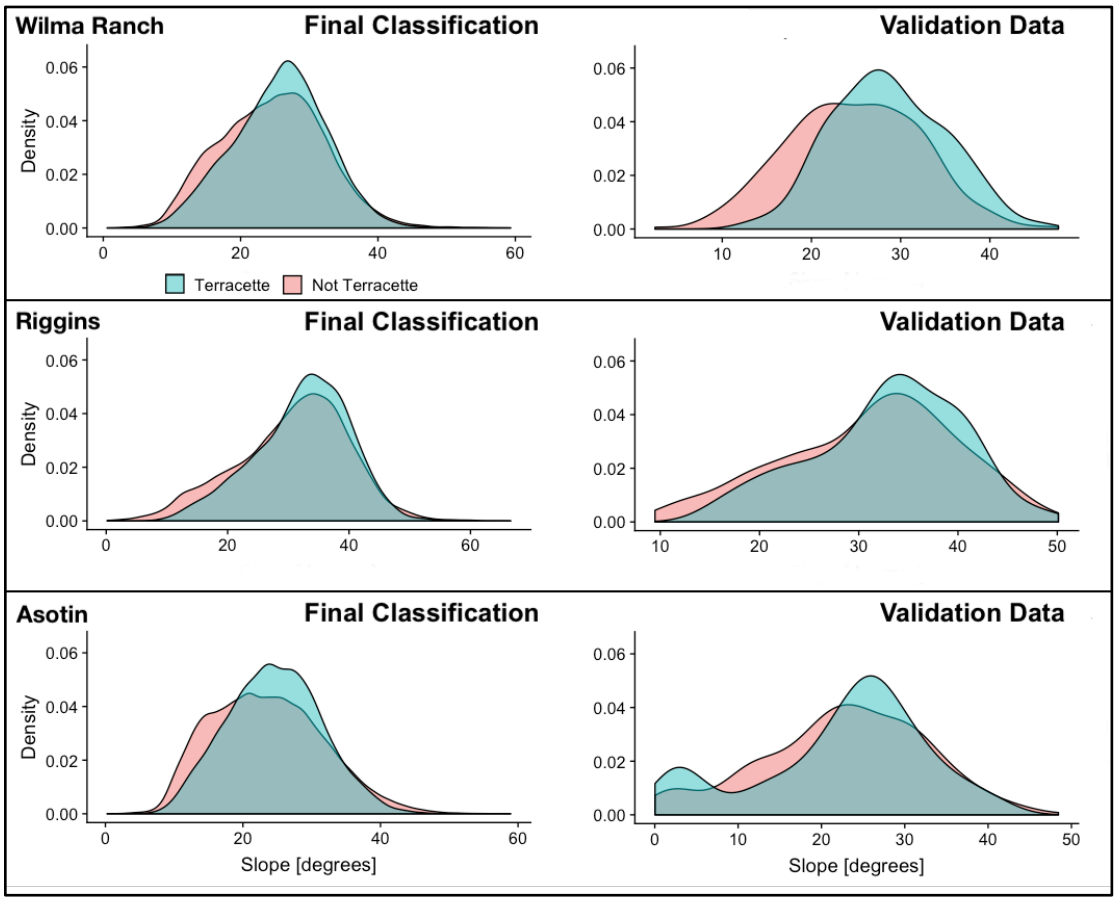

Figure 9. Density of slope for ground truth and final output estimation for all three study areas.

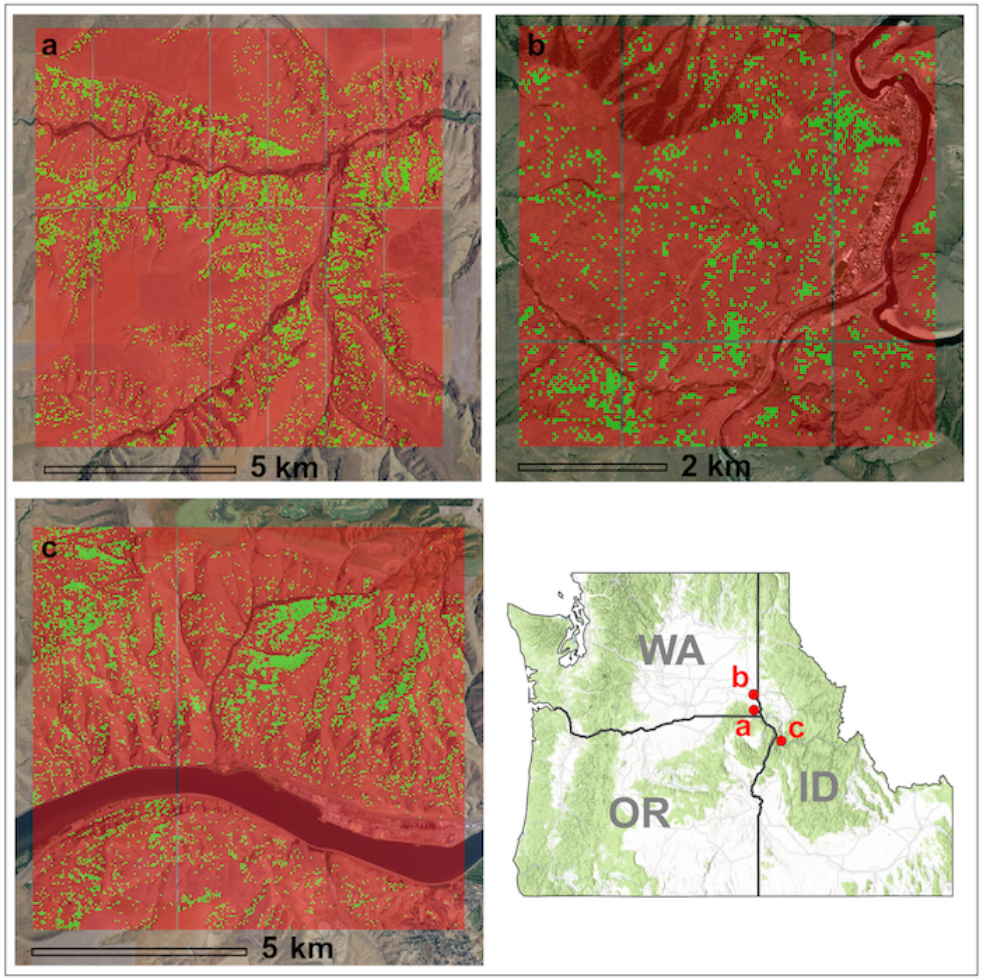

Figure 10. Results of final classification output for a) Asotin, b) Riggins and c) Wilma Ranch.

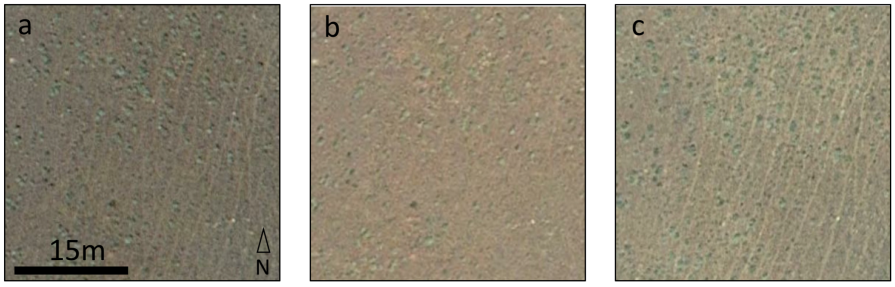

July 18, 2013 July 27, 2013 July 30, 2016

Figure 11. Unmodified images where *a* and *b* are archival imagery and *c* is from the imagery set used for this study. Here we see the effect that acquisition timing can have on terracette visibility. In *b*, taken only 9 days after *a*, the terracettes are not visible likely due to acquisition timing.

Table 1. Final balanced accuracy and Cohen's kappa for each classification. Omission and commission errors are shown for both terracette and not terracette classes. *Classifications had multiple radius and/or angular bandwidth combinations with the same balanced accuracy and kappa values.

Site & Method	Lower frequency limit (cycles / meter)	Upper frequency limit (cycles / meter)	Angular Bandwidth (degrees)	Balanced Accuracy	Kappa	Omission Terracette	Omission Not Terracette	Commission Terracette	Commission Not Terracette
Wilma Ranch* (Frequency only)	0.30 - 0.35	0.70	NA	0.76	0.52	0.35	0.20	0.22	0.29
Wilma Ranch* (Frequency+ Orientation)	0.21 - 0.30	0.70	55	0.78	0.57	0.30	0.22	0.22	0.26
Riggins* (Frequency only)	0.32	0.70 - 0.75	NA	0.76	0.51	0.33	0.16	0.19	0.28
Riggins* (Frequency + Orientation)	0.32	0.67 - 0.75	70	0.76	0.53	0.35	0.14	0.17	0.28
Asotin (Frequency only)	0.32	0.70	NA	0.77	0.54	0.29	0.16	0.19	0.26
Asotin* (Frequency + Orientation)	0.21 - 0.24	0.70 - 1.88	30 - 35	0.77	0.53	0.27	0.24	0.24	0.25
All Sites Combined (Frequency only)	0.32	0.70	NA	0.75	0.49	0.31	0.20	0.22	0.28
All Sites Combined* (Frequency + Orientation)	0.30	0.70	50 - 60	0.77	0.53	0.32	0.15	0.18	0.27

Table 2. Area values for digitized validation data zones and final, rule-based classification for terracettes and not terracettes classes. Suitable for terracette formation is defined here as areas with both slope between 5-60° and Grassland/Herbaceous and Shrub/Scrub landcover classification. *The Riggins site had gaps between images that resulted in the discrepancy in site area and final classification values.

	Asotin	**Riggins***	**Wilma**
Total site area (km^2)	56.0	16.0	45.0
Suitable for terracette development (km^2)	35.6	11.1	31.2
Manual Classification Zones			
Terracette (km^2)	2.2	1.0	5.7
Not Terracette (km^2)	53.8	15.0	39.3
Calculated Classification			
Terracette (km^2)	5.4	1.6	5.0
Not Terracette (km^2)	50.6	13.9	40.0